1-14-2020

Structural Analysis of Ultrasoft PDMS- g-PDMS Shell-Only Particles

Karin J. Bichler
Louisiana State University

Bruno Jakobi
Louisiana State University

Stefan O. Huber
Louisiana State University

Elliot P. Gilbert
Australian Centre for Neutron Scattering

Gerald J. Schneider
Louisiana State University

Recommended Citation

Bichler, K., Jakobi, B., Huber, S., Gilbert, E., & Schneider, G. (2020). Structural Analysis of Ultrasoft PDMS- g-PDMS Shell-Only Particles. *Macromolecules, 53* (1), 78-89. https://doi.org/10.1021/acs.macromol.9b01598

Structural analysis of ultra-soft PDMS-g-PDMS shell-only particles

Karin J. Bichler,[1*] Bruno Jakobi,[2] Stefan O. Huber,[1] Elliot P. Gilbert,[3] Gerald J. Schneider[1,2*]

[1]Department of Physics & Astronomy, Louisiana State University, Baton Rouge, LA 70803, United States

[2]Department of Chemistry, Louisiana State University, Baton Rouge, LA 70803, United States

[3]Australian Centre for Neutron Scattering, Australia Nuclear Science and Technology Organisation, Locked Bag 2001, Kirrawee DC, NSW 2232, Australia

Email address: kbichler@lsu.edu, gjschneider@lsu.edu

TOC picture

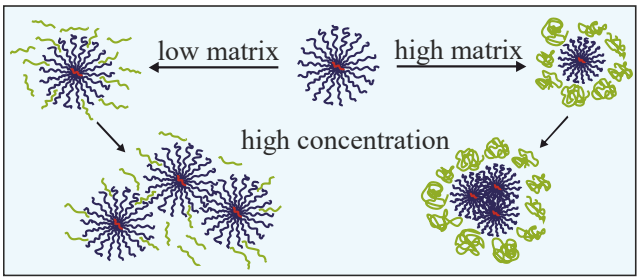

Abstract

We have used anionic polymerization to synthesize polymers of linear and bottlebrush architecture each with a polydimethylsiloxane backbone. The blending of polymer architectures has the effect of changing material properties, e.g. the viscoelasticity, which is connected to the chain conformation. Thus, we explore the conformation of bottlebrush polymers in a linear host melt both as a function of the concentration as well as for various molecular weights of the linear host matrices. Our bottlebrush polymers are seen as shell-only particles with a negligible core size. We

find a substantial influence of the molecular weight of the linear matrices on the structure of the bottlebrushes and their interactions. In samples with a low molecular weight matrix that has the same degree of polymerization as the side chains, the bottlebrush behavior is consistent with an effective theta solvent condition for all concentrations. With increasing molecular weight of the host matrix, this condition is only reached at the highest concentration of the bottlebrush polymers. The increase of the molecular weight of the host matrix leads to a shrinkage of the bottlebrushes and subsequently to a formation of clusters at higher volume concentrations. None of the scattering patterns show a pronounced correlation peak, however decreased forward scattering associated with a structure factor effect is observed.

Keywords

Bottlebrush, Shell-only particle, Star polymer, Colloid-cluster transition, Osmotic shrinkage

Introduction

Bottlebrush polymers are densely grafted macromolecules. They have gained significant attention in theoretical[1-5] and experimental works,[6-11] because of their architecture and resultant properties. The main structural features are the covalently bonded side chains on a backbone, which allows a manipulation of material properties, simply by changing the length of the side chains, the type of polymer used for the side chains, or the grafting density, *i.e.* ratio of side chains to backbone repeating units.[12] Applications include viscosity index manipulation,[13] supersoft elastomers[14-15] or photonic bandgap materials.[16-17] The overall shape of the bottlebrush polymer is driven by the ratio of the degree of polymerization (DP) of grafted side chains, DP_{sc}, compared to the backbone DP_{bb}. Bottlebrushes assume a spherical shape for $DP_{sc} > DP_{bb}$. By decreasing the side chain length, at a constant backbone length, a transition into a cylindrical or filament like

structure occurs.[8, 18] In the spherical region, the bottlebrush polymer is reminiscent of a star polymer (Figure 1).[19-20] From theory a star polymer is defined as a single molecule with chains attached to a central point. Experiments attempt to reach this definition as far as possible, but multi-arm star polymers require a finite sized core because of steric repulsion between the arms. A typical example is the utilization of a dendritic core.[21-22] The number arms that can be attached to a dendritic core are given by the functionality, which is directly related with the number of dendrimer generations. A multi-arm star polymer implies several generations which leads to a finite sized core.[19, 23] In comparison the core size of a bottlebrush is negligible, as illustrated in Figure ***1***. Therefore, spherical bottlebrush polymers are an ideal model system for soft particles. Due to the small core size, and the low dispersity of the side chains, the particles have a narrow dispersity. In comparison with polymer grafted nanoparticles (core-shell architecture),[24] these star-like polymer can be envisaged as shell-only particles.

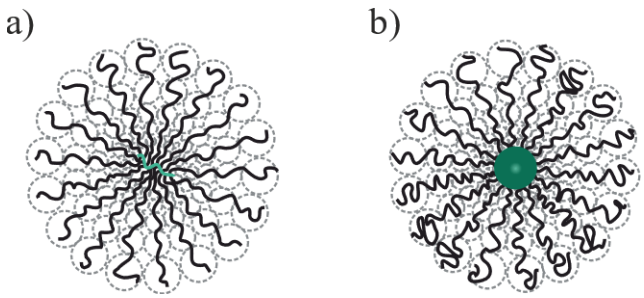

Figure 1: *Schematic comparison between a) spherical bottlebrush polymer and b) star polymer. The core of the bottlebrush polymer is vanishingly small compared to the core of the star polymer.*

In this paper we present a structural analysis of a spherical bottlebrush polymer dispersed in linear host matrices of varying molecular weights, measured by small angle neutron scattering (SANS). This mixture of architectures effectively represents shell-only particles immersed in linear polymer melts, allowing to study the molecular weight dependent changes on the morphology at the nano

and mesoscopic length scale of the shell. We focus on a solvent free system which is the limiting case for existing experiments in the literature on solutions of star polymers where linear chains are added to the system.[25-28] The molecular weight as well as the grafting density are determined by a combination of multi-angle light scattering gel-permeation chromatography (GPC-MALS) and nuclear magnetic resonance spectroscopy (NMR). SANS data have been analyzed using the random phase approximation (RPA) including a modified core-shell model and a Debye form factor, yielding information on the overall radius R of the bottlebrush polymer, the number of side chains f and the blob size ξ.

Theory

Model function for single particle form factor P(Q) – Modeling of the SANS data

The shape of bottlebrushes depends on the ratio of the degree of polymerization of the side chain, DP_{SC}, with that of the backbone, DP_{BB}. For $\frac{DP_{SC}}{DP_{BB}} \gg 1$, they assume a spherical structure.[29] For this case, the bottlebrush polymer can be approximated as a star polymer.[20, 30]

Form factor P(Q)

The total scattering intensity, $I(Q)$, is a product of the single particle form factor, $P(Q)$, describing the shape of the object and the structure factor $S(Q)$, which accounts for the interaction between neighboring particles. For monodisperse systems,

$$I(Q) \propto P(Q) \cdot S(Q) \tag{1}$$

whereby for dilute systems $S(Q) = 1$ and $I(Q) = P(Q)$ and can be described by a core-shell model initially derived for micelles and star polymers.[31-33] The scattering intensity is:

$$I(Q) = \frac{\Phi}{V_{total}} \cdot P(Q) \tag{2}$$

with the single particle form factor $P(Q)$ of chains attached to a core, following Pedersen[31] with "core" referring to the backbone, "shell" to the side chains, Φ to the volume concentration and V_{total} to the total volume with $V_{total} = f \cdot V_{shell} + V_{core}$.

$$\begin{aligned} P(Q) = {} & \Delta\rho_{core}^2 V_{core}^2 A(Q)_{core}^2 \\ & + 2f\Delta\rho_{core}\Delta\rho_{shell} V_{core} V_{shell} A(Q)_{core} A(Q)_{shell} \\ & + \Delta\rho_{shell}^2 V_{shell}^2 A(Q)_{shell}^2 f(f-1) \\ & + a \cdot f\Delta\rho_{shell}^2 V_{shell}^2 P(Q)_{blob} \end{aligned} \tag{3}$$

$\Delta\rho_{core} = \rho_{core} - \rho_{solvent}$ and $\Delta\rho_{shell} = \rho_{shell} - \rho_{solvent}$ describe the contrast of the core and the shell to the solvent, respectively. The constants ρ_{shell} and ρ_{core} are the scattering lengths densities of the shell and core. The volumes V_{core} and V_{shell} are defined as $V_i = \frac{M_{w_i}}{\varrho_i N_A}$ with the Avogadro constant $N_A = 6.022 \cdot 10^{23}$ mol^{-1}, weight average molecular weight M_{w_i} and mass density ϱ_i being associated with the core and the shell, and f denoting the number of side chains per molecule. The form factor of the blob scattering, P_{blob}, can be described with the Beaucage form factor[34] for arbitrary chain statistics, scaled with the prefactor a. It describes the internal chain conformation within the shell, where each side chain is composed of several blobs with increasing size by increasing radial dimension from the center to the outside. In this small region the polymer chain behaves as a Gaussian coil.[35]

$$P(Q)_{blob} = \exp\left(-\frac{Q^2\xi^2}{3}\right) + \left(\frac{d_f}{\xi^{d_f}}\right)\Gamma\left(\frac{d_f}{2}\right)\left(\frac{\operatorname{erf}\left(\frac{Qk\xi}{\sqrt{6}}\right)^3}{Q}\right)^{d_f} \tag{4}$$

Here, $k = 1.06$ is an empirical constant, ξ the radius of gyration and d_f the fractal dimension of the scattered particle which is typically $d_f = 2$ for melt or Θ-conditions. This parameter is connected to the Flory exponent ν with $d_f = 1/\nu$, giving the typical value of $\nu = 0.5$ for melt or Θ-condition.[36]

The normalized scattering amplitude of the core with a constant density profile can be written as:

$$A(Q)_{core} = \frac{3(\sin(QR_c) - (QR_c)\cos(QR_c))}{(QR_c)^3} \quad (5)$$

with R_c as the core radius.

The shell can be described with the normalized scattering amplitude $A(Q)_{shell}$ obtained by Fourier transformation of an explicit density profile.

$$A(Q)_{shell} = \frac{\int_{R_c}^{R} 4\pi r^2 \frac{\sin(Qr)}{Qr} \varphi(r)_{star} dr}{\int_{R_c}^{R} 4\pi r^2 \varphi(r)_{star} dr} \quad (6)$$

The shell dimension of our particles is finite, therefore we can use the overall radius R for the upper integration limit instead of ∞.

The star like density profile $\varphi(r)_{star}$ arises from the scaling theory for star polymers[35, 37] with a star consisting of three different regions (Figure 2): core, unswollen and swollen regions.

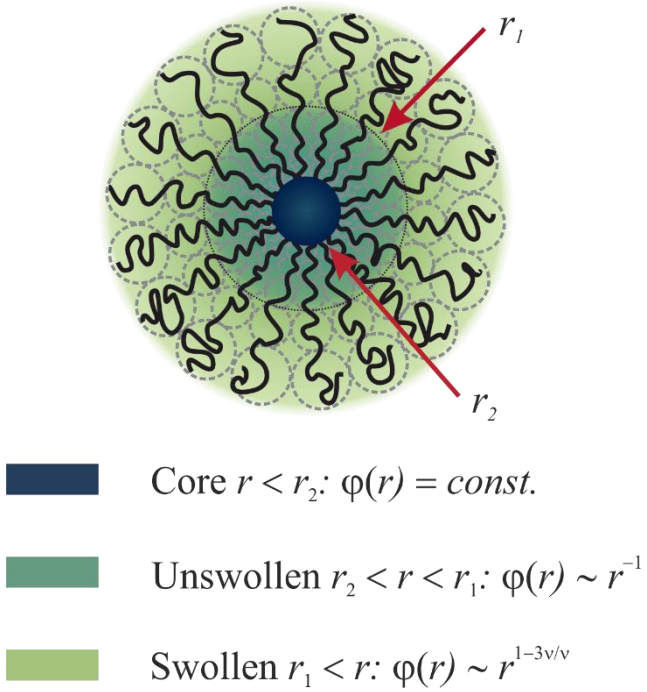

Figure 2: *Model for star like representation including blobs of three different density regions originating from scaling theory:*[35, 37] *Core, unswollen and swollen regions with* ν *being the Flory exponent:* $\nu = 0.588$ *for good solvent and* $\nu = 0.5$ *for Θ-condition.*

Our system comprises a polymer melt as matrix, giving a Θ-condition[38], with $\nu = 0.5$. By taking this Flory parameter into account, the swollen region reduces to $\varphi(r) \propto r^{-1}$ and merges together with the unswollen region. Therefore, only core and shell (unswollen region) are left. The shell can be described by the following density profile $\varphi(r)_{star}$: [39-40]

$$\varphi(r)_{star} = \frac{r^{-1}}{\left(1 + \exp\left(\frac{r - R}{\sigma R}\right)\right)} \tag{7}$$

Here the radial dependence of the monomer density distribution[41] is multiplied with the Fermi cut-off function to ensure a smooth density decay at R including the smearing parameter σ for averaging over all chains.

By considering the scattering lengths of each part of our (h-PDMS)-*g*-(d-PDMS) bottlebrush polymer with deuterated side chains, having protonated end groups at the dangling ends, we have three different contrasts (Figure 3a): core, shell and end group. By including every contrast into the form factor $P(Q)$ we have a core-shell-shell structure, where the second shell consists only of the end group contribution. However, the end group still belongs to the side chains which build up the shell of the bottlebrush polymer, just because of the different contrast we named it as a second "shell". The scattering intensities of the core and the end group shell is at least one order of magnitude weaker in comparison to that of the shell (Figure 3b).

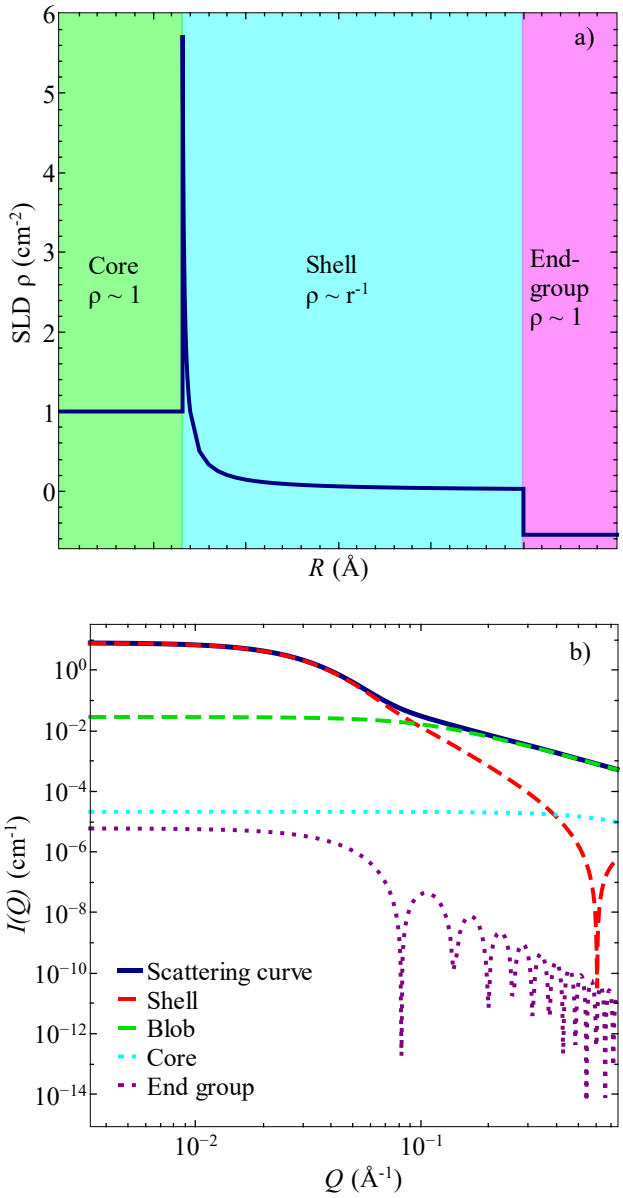

Figure 3: *a) Scattering length density ρ vs. radius R of the protonated core, the deuterated shell and the protonated end group. Core and end groups have a constant density profile, whereas the shell has a radial dependence based on scaling theory (equation 7). b) Scattering intensity, I(Q) vs momentum transfer Q of the model function together with the intensities from the individual contributions.*

132

Therefore, we can approximate the (h-PDMS)-g-(d-PDMS) bottlebrush by only considering the shell and the blob contribution. As the later analysis demonstrates, these two parts are sufficient to describe the whole scattering curve (*cf.* Results and Discussion section). Accordingly, the single particle form factor $P(Q)$, can be written as:

$$P(Q)_{BB} = \Delta\rho_{shell}^2 V_{shell}^2 A(Q)_{shell}^2 f(f-1) + a \cdot f \Delta\rho_{shell}^2 V_{shell}^2 P(Q)_{blob} \quad (8)$$

with the same expressions for the scattering amplitude as described earlier.

For systems composed of different architectures and different isotope labeling - here deuterated bottlebrush polymers and protonated linear chains - the random phase approximation (RPA) allows to weight all contributions including the interactions between them.

$$\frac{(\Delta\rho)^2}{I(Q)} = \frac{1}{\Phi_{BB} V_{BB} \tilde{P}(Q)_{BB}} + \frac{1}{\Phi_{LC} V_{LC} P(Q)_{Debye}} - 2\chi/V_0 \quad (9)$$

Here Φ_i and V_i correspond to the respective volume fraction and molecular volume of the bottlebrush polymer with $V_{BB} = f \cdot V_{shell}$ and the linear chains, V_0 is the geometric average monomer volume with $V_0 = \sqrt{V_H V_D}$ where V_H and V_D are the protonated and deuterated monomer volume respectively.[42] $P(Q)_{Debye}$ is the form factor of the linear chains of the host matrix and is given by the Debye formula

$$P(Q)_{Debye} = \frac{2}{\left(Q^2 R_g^2\right)^2} \left(Q^2 R_g^2 - 1 + \exp\left(-Q^2 R_g^2\right)\right) \quad (10)$$

with the radius of gyration R_g. R_g was calculated based on the relationship $\langle R_g^2 \rangle = \frac{1}{6} \langle R_{ee}^2 \rangle$ and the statistical segment length $b = 6.2$Å of PDMS, which was determined independently (*cf.* Supporting Info, Figure S1). For all modelling, R_g was fixed to theoretical values. The formfactor, used for considering the bottlebrush contribution changes from equation (8) to

$$\tilde{P}(Q)_{BB} = A(Q)^2_{shell}\frac{1}{f}(f-1) + a \cdot \frac{1}{f}\,P(Q)_{blob} \quad (11)$$

Most of the parameters presented above are calculated from the chemistry of the molecules. As seen in Figure 3a, the whole scattering curve can be described with the shell and the blob contribution only. Each part can be described with a set of two parameters independent of each other.

Materials and Methods

Synthesis

All reactions and manipulations were carried out under high vacuum or in a glovebox, with the oxygen and moisture level below 1 ppm, using standard high vacuum and Schlenk techniques.[43] All flasks were equipped with PTFE stopcocks to allow for high vacuum manipulation without the use of glassblowing. All chemicals and solvents were purchased from Millipore Sigma, except α,ω-divinyl-polydimethylsiloxane (DMS-V42) (Gelest Inc.) and purified as described below. Benzene was distilled and dried over a tert-butyl lithium – 1,1'diphenylethylene mixture and freshly distilled into the reaction flasks, THF was dried over CaH_2, distilled, dried over Na/K-benzopheneone and freshly distilled into the reaction flask before use. Hexamethylcyclotrisiloxane (D_3) was sublimated and dried in a 10 wt% solution of benzene over CaH_2, distilled, subsequently dried over tert-butyl lithium and distilled into the reaction flask prior to use. Deuterated hexamethylcyclotrisiloxane (D_3-*d18*) and octamethyltrisiloxane (D_4-*d24*) were synthesized following established procedures.[44-45] Further details can be found in the respective literature.[43-45]

Synthesis of host matrices:

The two low molecular weight matrices (lin-h-PDMS9k and lin-h-PDMS38k) were synthesized via kinetically controlled anionic ring opening polymerization (ROP) of D_3, initiated by lithium ehtynyldimethylsilanolate in a 50:50 mixture of benzene and tetrahydrofurane.[46] The polymerizations were terminated with chlorodimethylvinylsilane, dried, precipitated from toluene into methanol and dried under high vacuum. The lin-h-PDMS68k was fractionated from polydisperse PDMS via solution fractionation from a 1.5 volume percent solution in toluene through the addition of methanol as the third fraction and dried under high vacuum. The lin-d-PDMS3k was synthesized via cationic equilibrium ROP of D_4-*d24* with hexamethyldisiloxane and triflic acid.[47] All polymers are analyzed via GPC-MALS and ^{1}H NMR. The molecular weight, radius of gyration R_g and polydispersity M_w/M_n of the linear host matrices and the deuterated linear PDMS are summarized in Table 1.

Table 1: *Weight average molecular weight* $\boldsymbol{M_w}$*, number average molecular weight* $\boldsymbol{M_n}$*, polydispersity* $\boldsymbol{M_w/M_n}$ *and the calculated radius of gyration* $\boldsymbol{R_g^{calc}}$ *of the linear poly(dimethylsiloxane) (PDMS) polymer melt, used as the host matrix for the PDMS-g-PDMS bottlebrush polymer.* [a)]*Based on the statistical segment length of PDMS,* $\boldsymbol{b = 6.2}$ *Å. (cf. Supporting Info, Figure S1)*

Name	$\boldsymbol{M_w}$ (g/mol)	$\boldsymbol{M_n}$ (g/mol)	$\boldsymbol{M_w/M_n}$	$\boldsymbol{R_g^{calc}}$ (Å)[a)]
lin-h-PDMS9k	10600	8700	1.21	30.2
lin-h-PDMS38k	44700	38000	1.17	62.2
lin-h-PDMS68k	69400	68000	1.02	77.5
lin-d-PDMS3k	3600	3000	1.21	17.0

Synthesis of Bottlebrush PDMS-*g*-PDMS:

PDMS bottlebrushes were synthesized via the grafting-to method from living PDMS side chains onto a backbone with chlorosilane functionality (Figure 4).

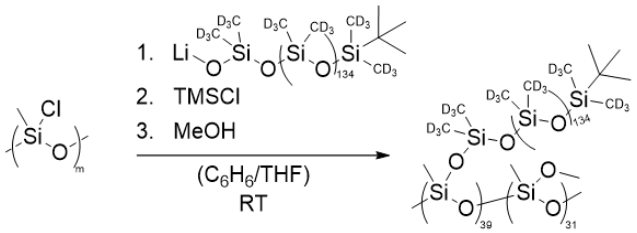

Figure 4: *Synthetic scheme towards PDMS bottlebrushes via a grafting-to method of living PDMS chains onto polychloromethylsiloxane.*

The backbone precursor, polymethylhydrosiloxane (PMHS), was synthesized via cationic equilibrium ROP of tetramethylcyclotetrasiloxane with tetramethyldisiloxane and trifilc acid, precipitated into acetonitrile and fractionated from dry toluene through addition of dry acetonitrile.[48] The seventh fraction was collected for use and dried under high vacuum. The backbone is activated through chlorination via an adapted method from Varaprath and Stutts.[49] Trichlorosiocycanuric acid was suspended in dichloromethane and PMHS in dichloromethane was added dropwise for a constant reflux. The reaction was stirred for two hours and then THF added dropwise for a constant reflux; the reaction was stirred overnight, dried under high vacuum and suspended in pentane. The suspension is filtered through a 220 µm PTFE filter membrane and dried, giving polychloromethylsiloxane (PClMS). The side chains were synthesized via kinetically controlled anionic ring opening polymerization (ROP) of D_3-*d18*, initiated by *tert*-lithium in a 50:50 mixture of benzene and tetrahydrofurane. After completion a small aliquot was taken for analysis and the remainder added to a solution of PClMS in benzene. The reaction was stirred for 20 h at 25 °C and terminated via the addition of chlorotrimethylsiloxane. After removal of all

solvents and precipitation from methanol into toluene, the resulting bottlebrush was received as the first fraction of the precipitative fractionation with toluene and methanol as solvent/non-solvent combination for the removal of free side chains. The molecular weights and polydispersity of side chain (d-PDMS), the backbone (h-PDMS), together with values for the whole (h-PDMS)-*g*-(d-PDMS) bottlebrush polymer are summarized in Table 2 (*cf.* Supporting Info, Figure S2). This gives a grafting density of side chains per backbone repeating unit of 56%, the residual free grafting sites were terminated with methoxy groups. This value is well above the threshold between comb and bottlebrush polymer.

Table 2: *Molecular weight M_n, degree of polymerization DP, and polydispersity $\boldsymbol{M_w/M_n}$, of the side chain (d-PDMS), the backbone (h-PDMS) and the (h-PDMS)-g-(d-PDMS) bottlebrush polymer.* [a)]*Per definition of a bottlebrush polymer.*

Name	$\mathbf{M_n}$ **(g/mol)**	$\mathbf{M_w}$ **(g/mol)**	**DP**	$\mathbf{M_w/M_n}$
Side chain	10800	11400	136	1.07
Backbone	4160	4230	70	1.02
Bottlebrush	404000	446000	70[a)]	1.10

Sample preparation:

PDMS-*g*-PDMS bottlebrush and linear host matrices were weighed into 1.5 mL vials on a 0.3 g total weight scale, dissolved in pentane, shaken for 24 h and dried under high vacuum.

Small-Angle Neutron Scattering (SANS)

Small-angle neutron scattering (SANS) experiments were carried out on the 40 m QUOKKA[50-51] instrument at the OPAL reactor at the Australian Nuclear Science and Technology Organization (ANSTO), Sydney, Australia. Three instrument configurations were used, two with equal source-to-sample and sample to detector distances of 20 and 8 m, and the final configuration with a source-to-sample distance of 12 m and a sample-detector distance of 1.3 m with a 300 mm lateral detector offset to increase the maximum accessible Q. Source and sample aperture diameters of 50 mm and 12.5 mm, respectively, were used. 5 Å neutrons ($\Delta\lambda/\lambda = 10\%$) were used at all of these configurations. These configurations provided a Q range of $0.003\ \text{Å}^{-1} < Q < 0.8\ \text{Å}^{-1}$ with the momentum transfer $Q = \frac{4\pi}{\lambda}\sin\left(\frac{\vartheta}{2}\right)$ and scattering angle ϑ. The data reduction was performed using the suite of NCNR SANS reduction macros[52], modified for the QUOKKA instrument, in the IGOR software package (Wave metrics, Oregon, US). After correction for empty cell scattering, transmission and detector response, the data were radially averaged and transformed onto an absolute scale by calibration with an attenuated direct beam. All samples were additionally background corrected, by subtracting the corresponding contributing volume fraction from the linear PDMS melt and incoherent scattering contribution.

Results and Discussion

Structural Analysis

We conducted SANS studies on the poly(dimethylsiloxane) (PDMS) bottlebrush polymer ((h-PDMS)-*g*-(d-PDMS)) in linear PDMS host matrices with molecular weight $M_n = 8700, 38000, \text{and } 68000$ g/mol - namely lin-h-PDMS9k, lin-h-PDMS38k, and lin-h-

PDMS68k - respectively. The intensities, divided by their respective bottlebrush concentration, are shown in Figure 5 and Figure 6.

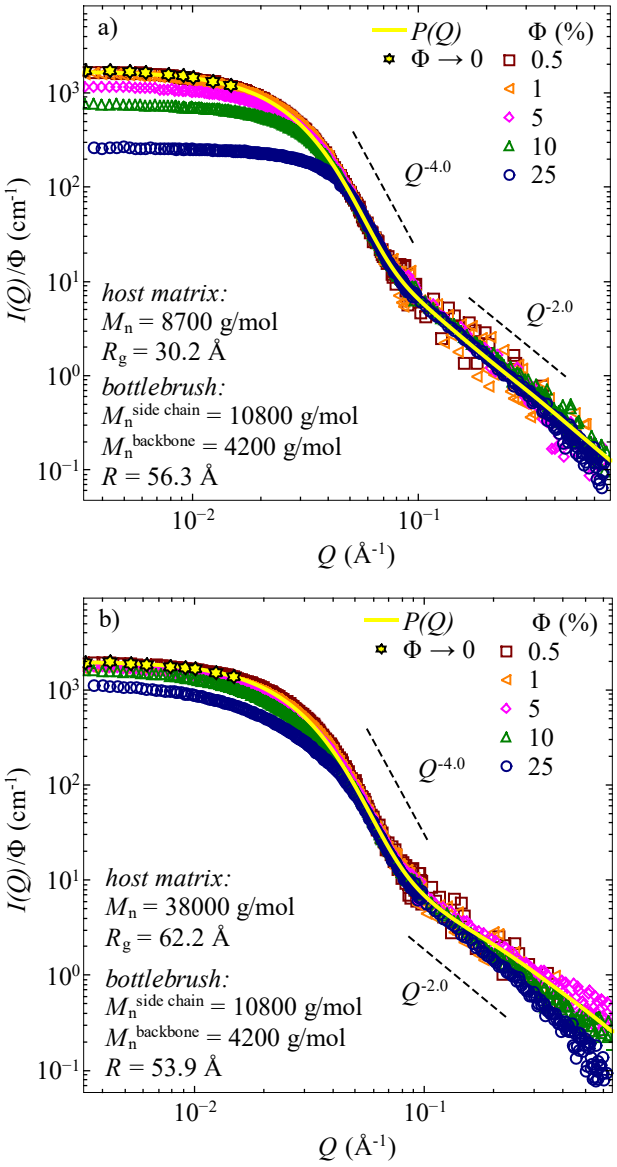

Figure 5: *Scattering intensities I(Q) vs. Q of PDMS-g-PDMS bottlebrush polymers in lin-h-PDMS9k (a) and lin-h-PDMS38k (b) matrices in double-logarithmic representation. Concentration series normalized to the respective volume fraction Φ including the extrapolated values that represent I(Φ = 0). The full cyan line represents a core-shell model used to describe*

the lowest scattering intensity $\Phi = 0.5\%$ based on equation (9). The errors are within the symbol size and not shown for clarity.

The scattering intensities of (h-PDMS)-*g*-(d-PDMS) bottlebrushes in lin-h-PDMS9k (Figure 5a), superimpose in the intermediate to high *Q*-region, but show substantial differences at the low *Q*. An extrapolation of the concentration series to $\Phi \to 0$ (yellow stars), by using $\Phi = 0.5\%, 1\%$, and 5%, indicates that there is a negligible or no structure factor $S(Q)$ contribution at the lowest measured volume fraction.[53]

This region of small momentum transfer is particularly sensitive to the structure factor, which would be visible as reduced forward scattering through a repulsive interaction. The scattering at the lowest concentration of $\Phi = 0.5\%$ is therefore consistent with the dilute regime enabling access to the particle form factor $P(Q)$.

The low *Q*-range corresponds to the Guinier region, whereas the intermediate Q^{-4} behavior reflects the Porod law. As seen in the scattering curve, the transition between Porod and Guinier region is not accompanied by an additional region of a different slope. This suggests that the structure of the PDMS based bottlebrushes is consistent with spherical objects. The Q^{-2} decay in the high *Q*-region is a signature of blob scattering,[35] whereby only the outermost blob is visible in SANS experiments.[54] One may therefore pose the question as to whether the size of the blobs changes with distance from the center. In order to tackle this question, we recall that the lin-h-PDMS9k matrix and the side chains of the bottlebrush have the same molecular weight. Therefore, we can assume that the mixture physically acts as a concentrated star solution, by considering the bottlebrushes and the linear chains together. This statement is based on the classification of Daoud *et al.*[35] which considers two regions - dilute and concentrated solutions - for scaling theory. These assumptions will be used further. Based on the scaling laws for this region (concentrated region),

all blobs have the same size once they start to overlap.[35, 37, 55] Additionally, the power law in the blob region observed in our experiments follows $Q^{-d_f} = Q^{-2}$. It is connected to the Flory exponent ν by $d_f = 1/\nu$. Therefore, the experimental $\nu = 0.5$ indicates a Θ-condition for all concentrations.

As illustrated in Figure 5b, increasing the molecular weight of the linear host matrix by a factor ~4 (38kg/mol, lin-h-PDMS38k) does not substantially affect the Q dependence of $P(Q)$, *i.e.*, the bottlebrush seems to stay spherical. At least at higher bottlebrush volume fractions, the spherical structure with smooth surface ($I \propto Q^{-4}$) is still maintained. A more detailed comparison with Figure 5a reveals that the concentration dependence changes, since the reduction of the forward scattering with increasing the concentration is less pronounced than observed in the short matrix (lin-h-PDMS9k). In the high Q-region, the power law changes with increasing concentration, but still reaches $d_f = 2$ at 25 %.

The change of the slope indicates a volume fraction-dependent solvent quality. In the lin-h-PDMS38k matrix the Θ-condition with $\nu = 1/2$ is only reached for the highest volume fraction, represented as a power law of Q^{-2}. This seems to be plausible because the mutual interpenetration of the side chains increases with increasing bottlebrush concentration. This leads to the fact that more chains of equal molecular weight interact. This is supported by measurements of the bottlebrushes in matrix chains of different molecular weights which exhibit a decrease of the solvent quality. The reduction of the solvent quality in the higher molecular weight matrix implies a greater tendency of the samples to form aggregates or different morphologies. Therefore, the structure factor would be less pronounced, though, there is no indication of aggregate formation or non-spherical structures in the experimental data. In order to explore this idea further, we continued to increase the molecular weight of the matrix chains.

In the next step we increase the molecular weight of the linear host matrix further, to 68 kg/mol, lin-h-PDMS68k, which is around 7 times larger than the molecular weight of the side chains (Figure 6).

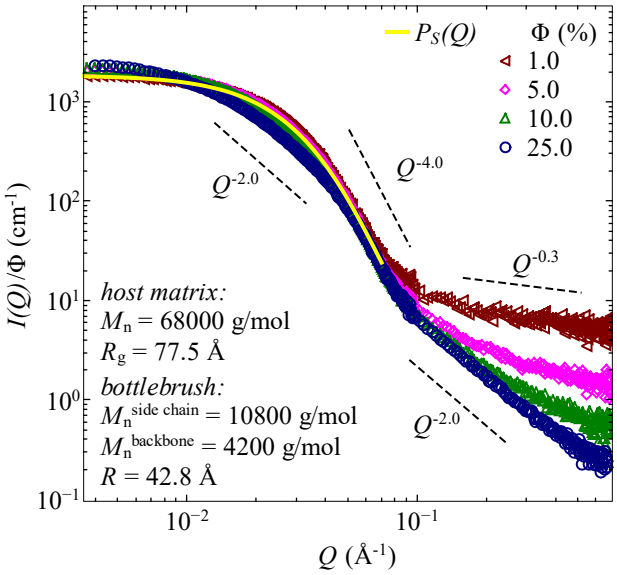

Figure 6: *Scattering intensities I(Q) vs. momentum transfer Q of PDMS-g-PDMS bottlebrush polymers in lin-h-PDMS68k matrix in a double logarithmic representation. Concentration series normalized to the respective volume fraction Φ. The full cyan line represents the description of the form factor for $\Phi = 1.0\%$ by only taking the shell contribution of our core-shell model (equation (9)).*

Most apparent is the almost vanishingly concentration dependence at low Q, and the strong dependence in the high Q-region which reaches a power law of Q^{-2} at the highest concentration. A more detailed inspection reveals the appearance of an additional power law Q^{-2} between the low and intermediate Q-region for $\Phi = 25\%$, the highest volume fraction of bottlebrushes. This suggest the starting point of clustering[25] or the formation of elongated objects, consisting of several bottlebrushes. Despite these obvious differences, the low concentration sample is very similar to

the cases in the low molecular weight matrices. In particular, we observe a direct transition from Guinier to Porod region, and the intensities are very similar, when compared to the bottlebrush in the lower molecular weight matrices. In this case the data modelling was done with $\Phi = 1.0\%$ (due to leaking sample of the $\Phi = 0.5\%$ during transport). Based on the behavior of the bottlebrush polymer in lin-h-PDMS9k and lin-h-PDMS38k, we assume that there is no contribution of the structure factor even at $\Phi = 1.0\%$ and the assumption of a pure form factor contribution is still satisfied.

Figure 7 illustrates the volume-normalized intensity at low Q-values to further explore the influence of the matrix chains on the structure factor. Our data point to a linear increase with the molecular weight of the host polymer, in a double-logarithmic plot. To a first order approximation, we obtain a power law, that has a strong relationship with the concentration, with an exponent that increases from 0.06 ± 0.004 (1%) to 1.0 ± 0.06 (25 %).

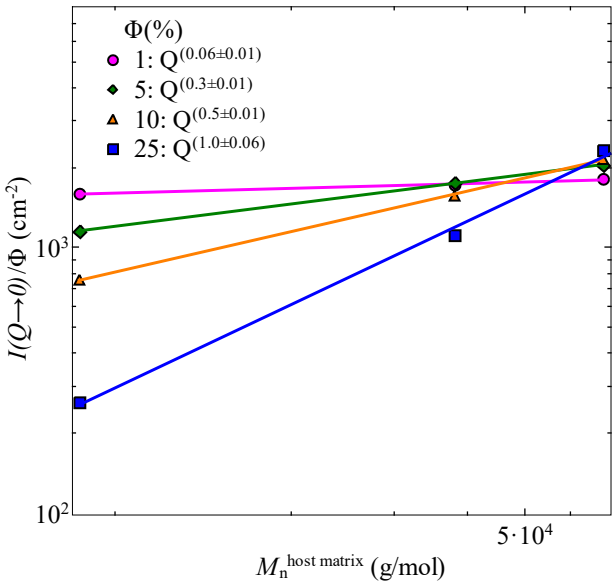

Figure 7: *Scattering intensity, $I(Q \to 0)$, divided by the bottlebrush concentration as a function of the molecular weight of the linear host matrix, for four concentrations of bottlebrushes, $\Phi = 1\%$, $\Phi = 5\%$, $\Phi = 10\%$ and $\Phi = 25\%$.*

The best model description of the experimental data can be achieved by a modified core shell model with a core of negligible size, used together with the random phase approximation (RPA) (equation (9)). The analysis supports our argument accompanying Figure 5 and Figure 6, that the samples with a low bottlebrush concentration can be well described by the particle form factor $P(Q)_{bb}$ only. This form factor only contains the shell and the blob contributions (equation (8)).

As expanded below, the density profile depends on the bottlebrush concentration and the host matrix molecular weight. Therefore, we calculate the average radius R_{avg} from the overall radius R, obtained by using the model function and the smearing parameter σ within the density profile $\varphi(r)_{star}$[56] (equation (7))

$$R_{avg} \coloneqq \frac{\int_0^R r^3 \cdot \varphi(r)_{star} dr}{\int_0^R r^2 \cdot \varphi(r)_{star} dr} \tag{12}$$

The best fit values for $\Phi = 0.5\%$ of lin-h-PDMS 9k and in lin-h-PDMS38k are summarized in Table 3 and for $\Phi = 1.0\%$ in Table 4. As Figure 8 illustrates, R_{avg} decreases linearly with increasing molecular weight of the host matrix. The average radius for the highest molecular weight is already identical with the anticipated value for the lowest limit radius R_{avg}^{low}. To estimate R_{avg}^{low} we assume that the minimum value of the mass density cannot be below the physical density $\varrho_{d-PDMS} = 1.02$ g/mol of linear deuterated PDMS. From $\varrho_{d-PDMS} = \frac{M}{V}$ with $M = M_w/N_A$, replacing V by the volume of a sphere, $V = \frac{4\pi}{3}(R_{avg}^{low})^3$ yields:

$$R_{avg}^{low} = \left(\frac{3}{4\pi N_A}\frac{M_w^{bottlebrush}}{\varrho_{d-PDMS}}\right)^{\frac{1}{3}} \tag{13}$$

By using equation (13) and taking $M_w^{bottlebrush}$ from Table 2, we find a value of $R_{avg}^{low} = 55.7$ Å. Based on the calculated value for the lower limit of the radius R_{avg}^{low}, the size obtained for the bottlebrush polymer in the highest molecular weight host matrix, lin-h-PDMS68k, is the smallest possible value for our system. This statement has a very important consequence because it defines an upper limit for the matrix molecular weight and thus a miscibility region in which the shell-only particles are miscible in linear polymer melts.

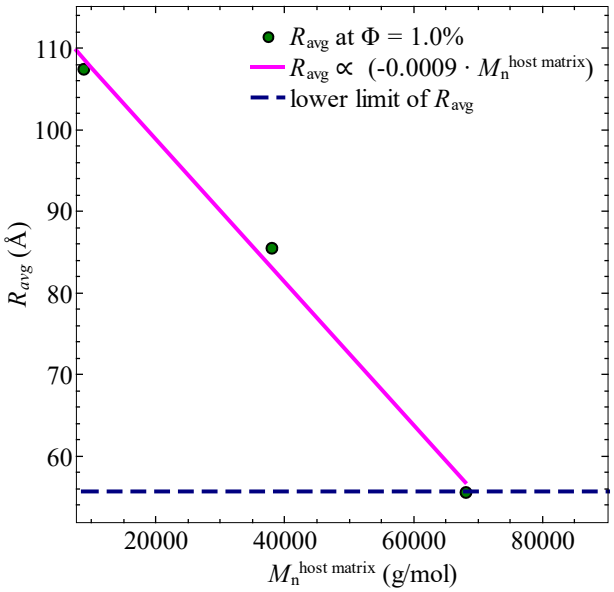

Figure 8: *Variation in average radius R_{avg} of the bottlebrushes with molecular weight of the host matrix including the lower limit of the average radius (dashed blue line), based on the density of pure deuterated PDMS.*

The associated Flory-Huggins interaction parameter χ, obtained by fitting the data with equation (9), are very small but increase with increasing molecular weight of the linear host matrix. However, the values are always negative. A similar trend is reported for polybutadiene star polymers with labeled single arms mixed in two linear host matrices with increasing molecular

weight.[57] In general, two components are only miscible if the χ-parameter is negative and additionally below the critical interaction parameter χ_{cr}.[58-59] The critical parameter can be calculated as

$$\chi_{cr} = \frac{1}{2} \cdot \left(\frac{1}{\sqrt{DP_{Bottlebrush}}} + \frac{1}{\sqrt{DP_{linear\ chains}}} \right)^2 \quad (14)$$

with $DP_{Bottlebrush}$ and $DP_{Linear\ chains}$ being the degree of polymerization of the bottlebrushes and the linear chains of the host matrices, respectively. It follows the same trend as the experimentally determined values. We note that equation (14) assumes mixtures of linear polymers. Therefore, we approximate $DP_{Bottlebrush}$ by twice the degree of polymerization of the side chains as the interacting segments, thus, $DP_{Bottlebrush} = 290$. The results are summarized in Table 5. All obtained values are below χ_{cr} and are therefore consistent with our experimental observations of miscibility.

Table 3: *Best fit values of the bottlebrush polymers, mixed with lin-h-PDMS9k and lin-h-PDMS38k, obtained by modeling the single particle form factor at the lowest concentration measured* $\boldsymbol{\Phi = 0.5\%}$. *All errors are smaller than 1%.*

Parameter	**lin-h-PDMS9k** $\boldsymbol{(\Phi = 0.5\%)}$	**lin-h-PDMS37k** $\boldsymbol{(\Phi = 0.5\%)}$
Overall Radius $\boldsymbol{R}$ (Å)	56.3	53.9
Radius of outermost blob $\boldsymbol{\xi}$ (Å)	14.2	8.7
Scaling parameter of blob $\boldsymbol{a}$	0.14	0.08
Smearing parameter $\boldsymbol{\sigma}$	0.36	0.39
Number of side chains $\boldsymbol{f}$	39.0	40.0

Average radius $\boldsymbol{R_{avg}}$ (Å)	107.5	97.9

Table 4: *Best fit values of all systems obtained by modeling the single particle form factor at* $\boldsymbol{\Phi = 1.0\%}$ *(cf. Supporting Info, Figure S3). For the largest host matrix, the blob size was not possible to determine. All errors are smaller than 1%.*

Parameter	**lin-h-PDMS9k** $\boldsymbol{(\Phi = 1.0\%)}$	**lin-h-PDMS37k** $\boldsymbol{(\Phi = 1.0\%)}$	**lin-h-PDMS68k** $\boldsymbol{(\Phi = 1.0\%)}$
Overall Radius $\boldsymbol{R}$ (Å)	53.6	53.1	42.8
Radius of outermost blob $\boldsymbol{\xi}$ (Å)	14.2	8.7	– – – –
Scaling parameter of blob $\boldsymbol{a}$	0.14	0.09	– – – –
Smearing parameter $\boldsymbol{\sigma}$	0.36	0.39	0.53
Number of side chains $\boldsymbol{f}$	39.0	40	40.0
Average radius $\boldsymbol{R_{avg}}$ (Å)	107.5	85.6	55.6

Table 5: *χ-parameter obtained from calculation and experiment for PDMS-g-PDMS bottlebrush polymer in linear host matrices with molecular weight of* $M_n = 8.7, 38, 68$ *kg/mol. The errors are smaller than 1% of the fit value.*

$\boldsymbol{\chi}$ **−parameter**	**lin-h-PDMS9k**	**lin-h-PDMS38k**	**lin-h-PDMS68k**
Experiment χ_{exp}	$-3.3 \cdot 10^{-3}$	$-1.1 \cdot 10^{-3}$	$-0.64 \cdot 10^{-3}$
critical χ_{cr}	$1.01 \cdot 10^{-2}$	$4.94 \cdot 10^{-3}$	$4.17 \cdot 10^{-3}$

In the next step we explore the concentration-dependent evolution of the structure factor. From its typical signatures, we only observe the lowered forward scattering. In Figure 5, a decrease of

the intensity with increasing bottlebrush concentration is seen; remarkably, increasing the molecular weight lowers this decrease. At the highest molecular weight, the decrease of the intensity is less pronounced or even disappeared. Moreover, in all cases the typical correlation peak, associated with the structure factor is absent in our systems.

Both observations (intensity and peak) could have two possible reasons, (i) smearing effect inherent to the polymer itself or (ii) reduction of the structure peak, known from star/linear polymer mixtures in solution.

Smearing is expected from the different contributions to the intensity in our samples. The main contrast is generated between the deuterated shell and the protonated linear chains of the host matrix. The contributions of the contrast between the protonated core and the protonated end groups of the deuterated side chains of our bottlebrush polymer are negligible for the form factor $P(Q)$ (Figure 3). However, they may influence the structure factor $S(Q)$, because of the additional contrast between the perimeter of the shell and the core. Ultimately, this can cause a broadening of the correlation peak until it is completely smeared.

Second, a similar behavior is known from star/linear polymer mixtures in solution.[13, 28, 60-62] If we assume that our system represents the limiting case without solvent, we can utilize the same underlying theory and attempt to explain our observations based on the respective interaction potentials. In such a mixture, three different interaction potentials are present: star – star V_{SS}, linear chains – linear chain V_{CC}, and linear chain – star V_{cs}

The star – star interaction can be described with an ultra-soft potential, which can be written as: [13, 55, 60, 63-65]

$$\beta V_{SS}(r) = \left(\frac{5}{18}\right) f^{\frac{3}{2}} \begin{cases} \left(\frac{1}{1+\frac{\sqrt{f}}{2}} - \ln\left(\frac{r}{\sigma_S}\right)\right) & \text{for } r \leq \sigma_S \\ \frac{1}{1+\frac{\sqrt{f}}{2}} \left(\frac{\sigma_S}{r}\right) \exp\left(-\frac{\sqrt{f}(r-\sigma_S)}{2\sigma_S}\right) & \text{for } r > \sigma_S \end{cases} \quad (15)$$

with f number of side chains, σ_S is the so-called corona diameter, equivalent to the star extension, r is the distance between two star centers, and $\beta = (k_B T)^{-1}$ where k_B is the Boltzmann constant and T the temperature. This potential has a logarithmic dependence at short distances ($r \leq \sigma_S$) and decays exponentially at long distances ($r > \sigma_S$). With increasing f, the transition to the typical hard sphere potential is established (Figure 9).

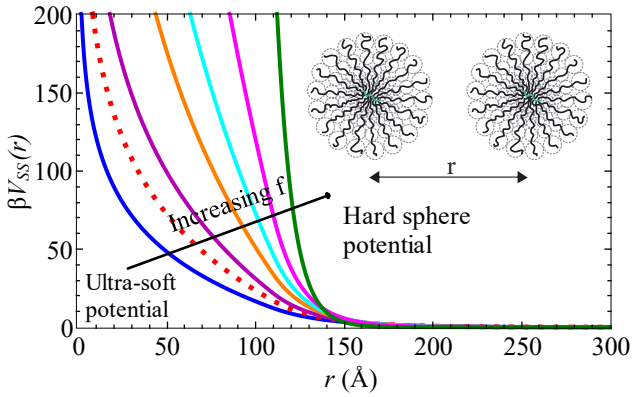

Figure 9: *Ultra-soft potential ranging to hard sphere potential for spherical bottlebrush polymer with outer perimeter of* $\sigma_b = 110$ Å *for different number of side chains* f. *From left to right:* $f = 30, 50, 75, 100, 150, and\ 500$. *The dotted red line represents our number of side chains* $f = 40$.

Additionally, the potential describing the interaction between two linear polymer chains V_{cc} is given by[60, 66]

$$\beta V_{cc}(r) = \left(\frac{5}{18}\right) f^{\frac{3}{2}} \begin{cases} \left(\frac{1}{2\tau^2\sigma_c^2} - \ln\left(\frac{r}{\sigma_c}\right)\right) & \text{for } r \leq \sigma_c \\ \frac{1}{2\tau^2\sigma_c^2}\exp\left(-\tau^2(r^2 - \sigma_c^2)\right) & \text{for } r > \sigma_c \end{cases} \quad (16)$$

This potential results from the star-star interaction potential, if the number of side chains is low ($f < 10$). The parameter σ_c measures the size of the polymer chain, r describes the distance between two linear chains by taking the middle monomeric unit as a center, and τ depends on the number of side chains and is a free parameter. From fitting of computer simulation data, $\tau = 1.03$ was determined for the case of a two-armed star polymer ($f = 2$), which reflects a linear chain.[66]

The star – chain interaction can be written as:[60]

$$\beta V_{sc}(r) = \begin{cases} -\Theta(f)\ln\left(\frac{r}{\sigma_{sc}}\right) + K & \text{for } r \leq \sigma_{sc} \\ \upsilon_0 \int \varphi(\boldsymbol{r}')_{star}\varphi(|\boldsymbol{r} - \boldsymbol{r}'|)_c d\boldsymbol{r}' & \text{for } r > \sigma_{sc} \end{cases} \quad (17)$$

with $\sigma_{sc} = \frac{1}{2}(\sigma_s + \sigma_c)$, $\Theta(f) = \frac{5}{36}\left(\frac{1}{\sqrt{2}-1}\right)\left[(f+2)^{\frac{3}{2}} - \left(f^{\frac{3}{2}} + 2^{\frac{3}{2}}\right)\right]$, K is a constant which can be evaluated by requiring continuity for $V_{sc}(r)$ and its first derivative at $r = \sigma_{sc}$, υ_0 is the excluded volume parameter and $\varphi(r)_{star}$ and $\varphi(r)_c$ are the radial dependent density profiles evaluated from the blob picture of the Daoud-Cotton model.[35]

The effective interaction potential of a star polymer dispersed in linear chains, resulting from the three different interaction potentials in the system is derived by Camargo *et al.*[26, 60, 67] and Mayer *et al.*[61]

In such a system, once linear chains are added, the pure star-star correlation is reduced due to the linear chains, which are occupying space between overlapping stars. This results in a decrease in the internal fluctuations. As seen in scattering diagrams, this effect is connected with a drastic decrease of the structure peak $S(Q)$ compared to a pure star polymer solution at higher concentration.[28]

The same effect is visible for spherical bottlebrush/linear polymer mixtures in d/h-toluene (Figure 10). Here we used protonated PDMS-*g*-PDMS bottlebrush polymers mixed with deuterated linear PDMS chains. The ratio of d/h toluene was chosen so that only the protonated bottlebrush polymer is visible and was determined by an initial SANS contrast variation experiment of deuterated linear PDMS chains (*cf.* Supporting Info, Figure S4).

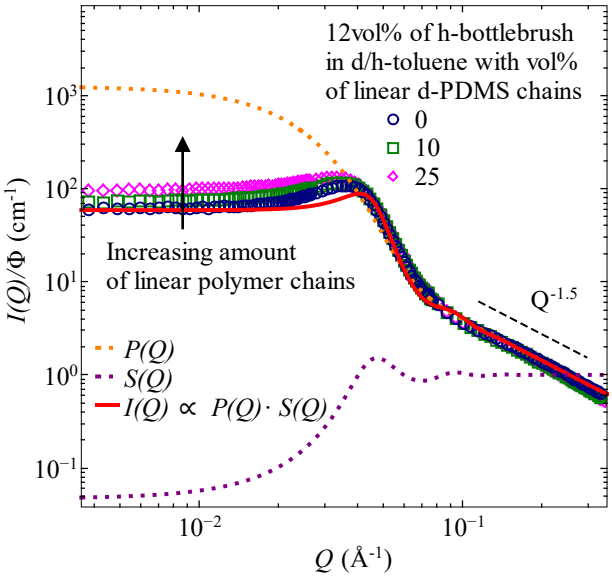

Figure 10: *Scattering intensity I(Q) vs. Q of PDMS-g-PDMS bottlebrush polymer in d/h-toluene solution with increasing volume fraction of deuterated linear PDMS chains, normalized to the volume fraction of bottlebrush polymers. The dashed green line represents a simulation of the single particle form factor P(Q), based on values for the same bottlebrush polymer in d-toluene. The dotted purple line represents the pure structure factor S(Q), obtained by using the ultra-soft potential. The red line represents the total scattering intensity, obtained by combining P(Q) and S(Q) for the mixture with* $\Phi = 0\%$ *of linear chains. The ratio of d/h-toluene was chosen based on the toluene–solvent contrast matching condition for deuterated PDMS.*

In a solution of protonated bottlebrush polymers in d/h toluene, a clear correlation peak in the intermediate Q-region is visible. This can be described with the form factor $P(Q)$ combined with the structure factor $S(Q)$. The latter one is obtained by solving the Ornstein-Zernike equation combined with the ultra-soft potential (equation (15)), as previously reported in the literature for star polymer solutions.[63] The theory differs slightly from the experimental data, which could come from the experimental resolution which is not included in the theory. By adding linear chains, the peaks become less obvious, especially with increasing concentration Φ (Figure 10), whereby the high Q-region follows the same power law, $Q^{-1.5}$, as the pure bottlebrush solution. The reduction in intensity of the structure peak is more pronounced by increasing the volume concentration of the added linear chains, or by increasing the molecular weight of the linear chains.[68]

The reduction in intensity of the correlation peak arises from a depletion-like phenomenon with the linear chains as the depletion agent. Further details can be found in the recent work by Stiakakis *et al.*[27] and Mayer *et al.*[61] The depletion effect was found to be extremely strong in melt compared to solvent for polymer nanocomposites and polymer/nanoparticle blends near a substrate.[69-71] The resulting osmotic force from the linear chains acts on the star polymers, especially seen by the changing size, depending on the molecular weight of the linear host matrix. For mixtures, with linear chains of approximately the same molecular weight, M_n, as one single arm, the star polymer will swell due to interpenetration with the arms. If the molecular weight of the linear chains increases, the star polymer will shrink induced by the osmotic pressure. Additionally, we hypothesize that with increasing molecular weight, the osmotic pressure exerted on the star polymer increases as well; this is supported by the decreasing size of the bottlebrush polymers by increasing the molecular weight of the linear host matrix. With increasing concentration of the bottlebrush polymers in the highest molecular weight host matrix, the osmotic

pressure forces the bottlebrushes closer together which subsequently leads to a formation of another structural level with non-spherical symmetry, which can be seen as the start of cluster formation.[25, 72] Similar behavior is known from polymer grafted nanoparticles. For polymer nanocomposites with $M_{matrix} \gg 2 \cdot M_{graft}$ the particle shell collapses and, subsequently, with increasing concentration of the polymer grafted nanoparticles, aggregation occurs.[73-74]

In solution a concentration dependence of the bottlebrush size was observed and predicted.[2, 53] This points our attention to the concentration dependent size. However, at high concentrations the analysis of the size is more difficult due to the dominant structure factor in the Guinier region. But the mid Q-region between $Q = 0.05 - 0.08\,\text{Å}^{-1}$ can be analyzed regarding size changes. A change in radius should shift the measured scattering towards higher or lower Q-values for shrinking or expanding radius, respectively, as illustrated by the simulation of different radii (*cf.* Supporting Info, Figure S5). Based on this assumption it can be concluded that the radius at this length scale is almost concentration independent, as even a change by 5 % is directly observable.

All these findings are summarized in Figure 11.

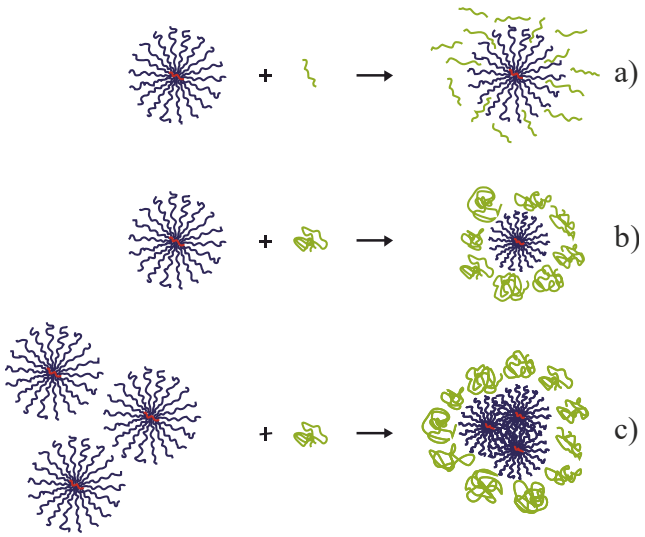

Figure 11: *Sketch of bottlebrush polymer mixed with linear chains of the same polymer: a) bottlebrush polymer in matrix of low molecular weight linear chains, b) bottlebrush polymer in matrix of high molecular weight linear chains, c) high concentration of bottlebrush polymers in matrix of high molecular weight linear chains.*

Conclusion

We have conducted small-angle neutron scattering experiments to understand the structural behavior of bottlebrush polymers dispersed in different linear polymer host environments. The form factor $P(Q)$ can be fully described by applying the random phase approximation to a modified core-shell model and the Debye form factor. For the high Q-region, a blob model, based on the Daoud-Cotton scaling theory for star polymers was used. For systems with bottlebrush polymer dispersed in lin-h-PDMS68k, the Daoud-Cotton model was unable to describe the data. The structure of the bottlebrush polymer is maintained over all molecular weights of the host matrix investigated. However, the overall radius decreases with increasing molecular weight of the host matrix polymer. Additionally, in the highest molecular weight host matrix, the bottlebrush polymers start to cluster with increasing bottlebrush concentration. This behavior is similar to

polymer grafted nanoparticles dispersed in a linear polymer melt and can be seen as a model system to obtain better insights in the behavior of the 'shell' only. In our system, a pronounced structure factor peak at higher concentrations is absent; however, the lowered forward scattering, which is associated with interparticle interactions, is present. This absence could be explained by either (i) the structure peak broadens due to smearing effects of the additional generated contrast between the protonated core and the protonated end groups in within the deuterated shell or (ii) the structure peak disappears because of a depletion-like phenomenon whereby the linear chains act as the depletion agents. According to the literature, the correlation between neighboring bottlebrushes is reduced. This effect is more pronounced with increasing molecular weight of the host matrix.

Acknowledgements

We acknowledge the support of Louisiana Consortium for Neutron Scattering (LaCNS). The neutron scattering work is supported by the U.S. Department of Energy (DoE) under EPSCoR Grant No. DE-SC0012432 with the additional support from the Louisiana Board of Regents. Additionally, the work is supported by the U.S. Department of Energy (DoE) under Grant No. DE-SC0019050. We would like to acknowledge ANSTO for access to the QUOKKA SANS instrument through proposal grant P6515 and FRMII for access to the KWSII SANS instrument.

Supporting Information Available:

The supporting information is available free of charge *via* the Internet at http://pubs.acs.org, including the results from the determination of the statistical segment length b, the GPC results,

the data description done at $\Phi = 1.0$ vol%, the contrast variation experiment, and the simulated scattering diagrams that would result from concentration dependent size changes.

References

1. Paturej, J.; Sheiko, S. S.; Panyukov, S.; Rubinstein, M., Molecular Structure of Bottlebrush Polymers in Melts. *Sci Adv* **2016,** *2* (11), e1601478.

2. Paturej, J.; Kreer, T., Hierarchical Excluded Volume Screening in Solutions of Bottlebrush Polymers. *Soft Matter* **2017,** *13*, 8534-8541.

3. Corsi, P.; Roma, E.; Gasperi, T.; Bruni, F.; Capone, B., Exploiting Scaling Laws for Designing Polymeric Bottle Brushes: A Theoretical Coarse-Graining for Homopolymeric Branched Polymers. *Phys Chem Chem Phys* **2019,** *21* (27), 14873-14878.

4. Fytas, N. G.; Theodorakis, P. E., Molecular Dynamics Simulations of Single-Component Bottle-Brush Polymers with Flexible Backbones under Poor Solvent Conditions. *J Phys Condens Matter* **2013,** *25* (28), 285105.

5. Cao, Z.; Carrillo, J.-M. Y.; Sheiko, S. S.; Dobrynin, A. V., Computer Simulations of Bottle Brushes: From Melts to Soft Networks. *Macromolecules* **2015,** *48* (14), 5006-5015.

6. Abbasi, M.; Faust, L.; Riazi, K.; Wilhelm, M., Linear and Extensional Rheology of Model Branched Polystyrenes: From Loosely Grafted Combs to Bottlebrushes. *Macromolecules* **2017,** *50* (15), 5964-5977.

7. Dalsin, S. J.; Hillmyer, M. A.; Bates, F. S., Linear Rheology of Polyolefin-Based Bottlebrush Polymers. *Macromolecules* **2015,** *48* (13), 4680-4691.

8. Pesek, S. L.; Li, X.; Hammouda, B.; Hong, K.; Verduzco, R., Small-Angle Neutron Scattering Analysis of Bottlebrush Polymers Prepared via Grafting-Through Polymerization. *Macromolecules* **2013,** *46* (17), 6998-7005.

9. Pesek, S. L.; Xiang, Q.; Hammouda, B.; Verduzco, R., Small-Angle Neutron Scattering Analysis of Bottlebrush Backbone and Side Chain Flexibility. *Journal of Polymer Science Part B: Polymer Physics* **2017,** *55* (1), 104-111.

10. Dutta, S.; Wade, M. A.; Walsh, D. J.; Guironnet, D.; Rogers, S. A.; Sing, C. E., Dilute Solution Structure of Bottlebrush Polymers. *Soft Matter* **2019,** *15* (14), 2928-2941.

11. López-Barrón, C. R.; Tsou, A. H.; Hagadorn, J. R.; Throckmorton, J. A., Highly Entangled α-Olefin Molecular Bottlebrushes: Melt Structure, Linear Rheology, and Interchain Friction Mechanism. *Macromolecules* **2018,** *51* (17), 6958-6966.

12. Sheiko, S. S.; Sumerlin, B. S.; Matyjaszewski, K., Cylindrical Molecular Brushes: Synthesis, Characterization, and Properties. *Progress in Polymer Science* **2008,** *33* (7), 759-785.

13. Likos, C. N., Soft Matter with Soft Particles. *Soft Matter* **2006,** *2* (6), 478-498.

14. Daniel, W. F.; Burdynska, J.; Vatankhah-Varnoosfaderani, M.; Matyjaszewski, K.; Paturej, J.; Rubinstein, M.; Dobrynin, A. V.; Sheiko, S. S., Solvent-Free, Supersoft and Superelastic Bottlebrush Melts and Networks. *Nat Mater* **2016,** *15* (2), 183-9.

15. Pakula, T.; Zhang, Y.; Matyjaszewski, K.; Lee, H.-i.; Boerner, H.; Qin, S.; Berry, G. C., Molecular Brushes as Super-Soft Elastomers. *Polymer* **2006,** *47* (20), 7198-7206.

16. Miyake, G. M.; Piunova, V. A.; Weitekamp, R. A.; Grubbs, R. H., Precisely Tunable Photonic Crystals from Rapidly Self-Assembling Brush Block Copolymer Blends. *Angew Chem Int Ed Engl* **2012,** *51* (45), 11246-8.

17. Miyake, G. M.; Weitekamp, R. A.; Piunova, V. A.; Grubbs, R. H., Synthesis of Isocyanate-Based brush Block Copolymers and Their Rapid Self-Assembly to Infrared-Reflecting Photonic Crystals. *J Am Chem Soc* **2012,** *134* (34), 14249-54.

18. López-Barrón, C. R.; Brant, P.; Eberle, A. P.; Crowther, D. J., Linear Rheology and Structure of Molecular Bottlebrushes with Short Side Chains. *Journal of Rheology* **2015,** *59* (3), 865-883.

19. Snijkers, F.; Cho, H. Y.; Nese, A.; Matyjaszewski, K.; Pyckhout-Hintzen, W.; Vlassopoulos, D., Effects of Core Microstructure on Structure and Dynamics of Star Polymer Melts: from Polymeric to Colloidal Response. *Macromolecules* **2014,** *47* (15), 5347-5356.

20. Levi, A. E.; Lequieu, J.; Horne, J. D.; Bates, M. W.; Ren, J. M.; Delaney, K. T.; Fredrickson, G. H.; Bates, C. M., Miktoarm Stars via Grafting-Through Copolymerization: Self-Assembly and the Star-to-Bottlebrush Transition. *Macromolecules* **2019,** *52* (4), 1794-1802.

21. Vasilenko, N.; Ignat'eva, G.; Myakushev, V.; Rebrov, E.; Moeller, M.; Muzafarov, A. In *Functional Multiarm Star Polydimethylsiloxanes*, Doklady Chemistry, Springer: 2001; pp 84-88.

22. Ren, J. M.; McKenzie, T. G.; Fu, Q.; Wong, E. H.; Xu, J.; An, Z.; Shanmugam, S.; Davis, T. P.; Boyer, C.; Qiao, G. G., Star Polymers. *Chem Rev* **2016,** *116* (12), 6743-836.

23. Maiti, P. K.; Çağın, T.; Wang, G.; Goddard, W. A., Structure of PAMAM Dendrimers: Generations 1 Through 11. *Macromolecules* **2004,** *37* (16), 6236-6254.

24. Mark, C.; Holderer, O.; Allgaier, J.; Hubner, E.; Pyckhout-Hintzen, W.; Zamponi, M.; Radulescu, A.; Feoktystov, A.; Monkenbusch, M.; Jalarvo, N.; Richter, D., Polymer Chain Conformation and Dynamical Confinement in a Model One-Component Nanocomposite. *Phys Rev Lett* **2017,** *119* (4), 047801.

25. Wilk, A.; Huissmann, S.; Stiakakis, E.; Kohlbrecher, J.; Vlassopoulos, D.; Likos, C. N.; Meier, G.; Dhont, J. K.; Petekidis, G.; Vavrin, R., Osmotic Shrinkage in Star/Linear Polymer Mixtures. *Eur Phys J E Soft Matter* **2010,** *32* (2), 127-34.

26. Camargo, M.; Likos, C. N., Phase Separation in Star-Linear Polymer Mixtures. *J Chem Phys* **2009,** *130* (20), 204904.

27. Stiakakis, E.; Vlassopoulos, D.; Likos, C. N.; Roovers, J.; Meier, G., Polymer-Mediated Melting in Ultrasoft Colloidal Gels. *Phys Rev Lett* **2002,** *89* (20), 208302.

28. Lonetti, B.; Camargo, M.; Stellbrink, J.; Likos, C. N.; Zaccarelli, E.; Willner, L.; Lindner, P.; Richter, D., Ultrasoft Colloid-Polymer Mixtures: Structure and Phase diagram. *Phys Rev Lett* **2011,** *106* (22), 228301.

29. López-Barrón, C. R.; Brant, P.; Eberle, A. P. R.; Crowther, D. J., Linear Rheology and Structure of Molecular Bottlebrushes with Short Side Chains. *Journal of Rheology* **2015,** *59* (3), 865-883.

30. Denesyuk, N. A., Bottle-Brush Polymers as an Intermediate Between Star and Cylindrical Polymers. *Physical Review E* **2003,** *68* (3), 031803.

31. Pedersen, J. S., Analysis of Small-Angle Scattering Data from Colloids and Polymer Solutions: Modeling and Least-Squares Fitting. *Advances in Colloid and Interface Science* **1997,** *70*, 171-210.

32. Pedersen, J., Small-Angle Scattering from Surfactants and Block Copolymer Micelles. In *Soft Matter Characterization*, Springer: 2008; pp 191-233.

33. Lund, R.; Pipich, V.; Willner, L.; Radulescu, A.; Colmenero, J.; Richter, D., Structural and Thermodynamic Aspects of the Cylinder-to-Sphere Transition in Amphiphilic Diblock Copolymer Micelles. *Soft Matter* **2011,** *7* (4), 1491-1500.

34. Beaucage, G., Small-Angle Scattering from Polymeric Mass Fractals of Arbitrary Mass-Fractal Dimension. *Journal of Applied Crystallography* **1996,** *29* (2), 134-146.

35. Daoud, M.; Cotton, J. P., Star Shaped Polymers : A Model for the Conformation and its Concentration Dependence. *J. Phys. France* **1982,** *43* (3), 531-538.

36. Dozier, W. D.; Huang, J. S.; Fetters, L. J., Colloidal Nature of Star Polymer Dilute and Semidilute Solutions. *Macromolecules* **1991,** *24* (10), 2810-2814.

37. Grest, G. S.; Fetters, L. J.; Huang, J. S.; Richter, D., Star polymers: Experiment, Theory, and Simulation. *Advances in Chemical Physics: Polymeric Systems* **1996,** *94*, 67-163.

38. Strobl, G. R., *The Physics of Polymers: Concepts for Understanding Their Structures and Behavior*. Springer Berlin Heidelberg: 2013.

39. Gupta, S.; Camargo, M.; Stellbrink, J.; Allgaier, J.; Radulescu, A.; Lindner, P.; Zaccarelli, E.; Likos, C. N.; Richter, D., Dynamic Phase Diagram of Soft Nanocolloids. *Nanoscale* **2015,** *7* (33), 13924-34.

40. Lund, R.; Willner, L.; Monkenbusch, M.; Panine, P.; Narayanan, T.; Colmenero, J.; Richter, D., Structural Observation and Kinetic Pathway in the Formation of Polymeric Micelles. *Phys Rev Lett* **2009,** *102* (18), 188301.

41. Daoud, M.; Joanny, J. F., Conformation of Branched Polymers. *Journal de Physique* **1981,** *42* (10), 1359-1371.

42. Arrighi, V.; Gagliardi, S.; Dagger, A. C.; Semlyen, J. A.; Higgins, J. S.; Shenton, M. J., Conformation of Cyclics and Linear Chain Polymers in Bulk by SANS. *Macromolecules* **2004,** *37* (21), 8057-8065.

43. Hadjichristidis, N.; Iatrou, H.; Pispas, S.; Pitsikalis, M., Anionic Polymerization: High Vacuum Techniques. *Journal of Polymer Science Part A: Polymer Chemistry* **2000,** *38* (18), 3211-3234.

44. Beltzung, M.; Picot, C.; Rempp, P.; Herz, J., Investigation of the Conformation of Elastic Chains in Poly (dimethylsiloxane) Networks by Small-Angle Neutron Scattering. *Macromolecules* **1982,** *15* (6), 1594-1600.

45. Willner, L.; Lund, R.; Monkenbusch, M.; Holderer, O.; Colmenero, J.; Richter, D., Polymer Dynamics Under Soft Confinement in a Self-Assembled System. *Soft Matter* **2010,** *6* (7).

46. Bellas, V.; Iatrou, H.; Hadjichristidis, N., Controlled Anionic Polymerization of Hexamethylcyclotrisiloxane. Model Linear and Miktoarm Star Co- and Terpolymers of Dimethylsiloxane with Styrene and Isoprene. *Macromolecules* **2000,** *33* (19), 6993-6997.

47. Chojnowski, J.; Wilczek, L., Mechanism of the Polymerization of Hexamethylcyclotrisiloxane (D3) in the Presence of a Strong Protonic Acid. *Die Makromolekulare Chemie* **1979,** *180* (1), 117-130.

48. Gupta, S. P.; Moreau, M.; Masure, M.; Sigwalt, P., Cationic Polymerization of 1,3,5,7 Tetramethylcyclotetrasiloxane Initiated by Ttrifluoromethanesulphonic Acid. *European Polymer Journal* **1993,** *29* (1), 15-22.

49. Varaprath, S.; Stutts, D. H., Utility of Trichloroisocyanuric Acid in the Efficient Chlorination of Silicon Hydrides. *Journal of Organometallic Chemistry* **2007,** *692* (10), 1892-1897.

50. Gilbert, E. P.; Schulz, J. C.; Noakes, T. J., 'Quokka'—The Small-Angle Neutron Scattering Instrument at OPAL. *Physica B: Condensed Matter* **2006,** *385-386*, 1180-1182.

51. Wood, K.; Mata, J. P.; Garvey, C. J.; Wu, C.-M.; Hamilton, W. A.; Abbeywick, P.; Bartlett, D.; Bartsch, F.; Baxter, P.; Booth, N.; al., e., QUOKKA, the Pinhole Small-Angle Neutron Scattering Instrument at the OPAL Research Reactor, Australia: Design, Performance, Operation and Scientific Highlights. *Journal of Applied Crystallography* **2018,** *51* (2), 294-314.

52. Kline, S. R., Reduction and Analysis of SANS and USANS Data Using IGOR Pro. *Journal of Applied Crystallography* **2006,** *39* (6), 895-900.

53. Bolisetty, S.; Rosenfeldt, S.; Rochette, C. N.; Harnau, L.; Lindner, P.; Xu, Y.; Muller, A. H.; Ballauff, M., Interaction of Cylindrical Polymer Brushes in Dilute and Semi-Dilute Solution. *Colloid Polym Sci* **2009,** *287* (2), 129-138.

54. Rathgeber, S.; Pakula, T.; Wilk, A.; Matyjaszewski, K.; Beers, K. L., On the Shape of Bottle-Brush Macromolecules: Systematic Variation of Architectural Parameters. *J Chem Phys* **2005,** *122* (12), 124904.

55. Likos, C. N., Effective Interactions in Soft Condensed Matter Physics. *Physics Reports* **2001,** *348* (4-5), 267-439.

56. Kalb, J.; Dukes, D.; Kumar, S. K.; Hoy, R. S.; Grest, G. S., End Grafted Polymernanoparticles in a Polymeric Matrix: Effect of Coverage and Curvature. *Soft Matter* **2011,** *7* (4), 1418-1425.

57. Richards, R. W., Influence of Architecture on Arm Dimensions and Interaction Parameters in Polybutadiene Star Polymers. *Macromolecules* **1999,** *32* (3), 880-891.

58. Andersen, B. Investigations on Environmental Stress Cracking Resistance of LDPE/EVA Blends. Dissertation, Martin-Luther-Universität Halle-Wittenberg, Halle-Wittenberg, 2004.

59. Manias, E.; Utracki, L. A., Thermodynamics of Polymer Blends. In *Polymer Blends Handbook*, Utracki, L. A.; Wilkie, C. A., Eds. Springer Netherlands: Dordrecht, 2014; pp 171-289.

60. Camargo, M.; Likos, C. N., Unusual Features of Depletion Interactions in Soft Polymer-Based Colloids Mixed with Linear Homopolymers. *Phys Rev Lett* **2010,** *104* (7), 078301.

61. Mayer, C.; Likos, C. N., A Coarse-Grained Description of Star−Linear Polymer Mixtures. *Macromolecules* **2007,** *40* (4), 1196-1206.

62. Stiakakis, E.; Petekidis, G.; Vlassopoulos, D.; Likos, C. N.; Iatrou, H.; Hadjichristidis, N.; Roovers, J., Depletion and Cluster Formation in Soft Colloid - Polymer Mixtures. *EPL (Europhysics Letters)* **2005,** *72* (4), 664.

63. Likos, C. N.; Löwen, H.; Watzlawek, M.; Abbas, B.; Jucknischke, O.; Allgaier, J.; Richter, D., Star Polymers Viewed as Ultrasoft Colloidal Particles. *Physical Review Letters* **1998,** *80* (20), 4450-4453.

64. Likos, C. N.; Mayer, C.; Stiakakis, E.; Petekidis, G., Clustering of Soft Colloids due to Polymer Additives. *Journal of Physics: Condensed Matter* **2005,** *17* (45), S3363-S3369.

65. Watzlawek, M.; Löwen, H.; Likos, C. N., The Anomalous Structure Factor of Dense Star Polymer Solutions. *Journal of Physics: Condensed Matter* **1998,** *10* (37), 8189-8205.

66. Jusufi, A.; Dzubiella, J.; Likos, C. N.; Ferber, C. v.; Löwen, H., Effective Interactions Between Star Polymers and Colloidal Particles. *Journal of Physics: Condensed Matter* **2001,** *13* (28), 6177-6194.

67. Camargo, M.; Egorov, S. A.; Likos, C. N., Cluster Formation in Star-Linear Polymer Mixtures: Equilibrium and Dynamical Properties. *Soft Matter* **2012,** *8* (15), 4177-4184.

68. Vlassopoulos, D., Colloidal Star Polymers: Models for Studying Dynamically Arrested States in Soft Matter. *Journal of Polymer Science Part B: Polymer Physics* **2004,** *42* (16), 2931-2941.

69. Padmanabhan, V.; Frischknecht, A. L.; Mackay, M. E., Effect of Chain Stiffness on Nanoparticle Segregation in Polymer/Nanoparticle Blends Near a Substrate. *Macromolecular Theory and Simulations* **2012,** *21* (2), 98-105.

70. Hooper, J. B.; Schweizer, K. S.; Desai, T. G.; Koshy, R.; Keblinski, P., Structure, Surface Excess and Effective Interactions in Polymer Nanocomposite Melts and Concentrated Solutions. *J Chem Phys* **2004,** *121* (14), 6986-97.

71. Ganesan, V.; Jayaraman, A., Theory and Simulation Studies of Effective Interactions, Phase Behavior and Morphology in Polymer Nanocomposites. *Soft Matter* **2014,** *10* (1), 13-38.

72. Vlassopoulos, D.; Stiakakis, E.; Kapnistos, M., Model Soft Colloids Out of Equilibrium: Glass-Like and Re-Entrant Transitions. *Rheol. Rev* **2007**, 179-252.

73. Rizk, M.; Krutyeva, M.; Lühmann, N.; Allgaier, J.; Radulescu, A.; Pyckhout-Hintzen, W.; Wischnewski, A.; Richter, D., A Small-Angle Neutron Scattering Study of a Soft Model Nanofiller in an Athermal Melt. *Macromolecules* **2017,** *50* (12), 4733-4741.

74. Wang, X.; Foltz, V. J.; Rackaitis, M.; Böhm, G. G. A., Dispersing Hairy Nanoparticles in Polymer Melts. *Polymer* **2008,** *49* (26), 5683-5691.